Combined convection flow in a vertical duct with wall temperatures that vary linearly with depth

A. T. Jones and D. B. Ingham
Department of Applied Mathematical Studies, Leeds University, Leeds, UK

Numerical solutions are presented for the problem of steady laminar combined convection flows in vertical parallel-plate ducts, with linearly varying wall temperatures. Neglecting streamwise diffusion in the analysis leads to a parabolic set of governing equations. These are solved using a marching technique for an implicit finite-difference scheme with vorticity, streamfunction, and temperature as independent variables. Various values of the governing parameter, the Grashof number, Gr, are considered, including the forced convection solution, $Gr = 0$, while the Prandtl number, Pr, is set at a value of unity in order to present the numerical method. As the value of $|Gr|$ increases, reverse flow regions appear that are present in the fully-developed flow; these are dealt with using a modification of the standard marching technique. Results are obtained in terms of velocity profiles, local Nusselt numbers, flow average temperatures, and friction factors, and the comparative strengths of the recirculation regions are assessed. A simple correlation is given for the development lengths, in terms of Gr, for $Pr = 1$.

Keywords: combined convection; vertical duct; reverse flows

Introduction

The problem of obtaining numerical solutions for mixed convection flows between vertical parallel plates where the temperature on the walls varies linearly with height is relevant to, for example, the modeling of oil wells, which can be considered to be ducts subjected to a geothermal gradient. In practice such problems may involve three-dimensional (3-D) geometries, annular flows, and complicated rheological properties of the multiphase fluids. However, a first approximation is required for the problem that exhibits some of the important properties of the full model. Hence, in order to develop the numerical methods required, a parallel-plate geometry is used. Previous studies of developing flows have concentrated on the forced convection case, although Ostrach (1954), Morton (1960), and Beckett (1980), among others, studied the kinematically and thermally fully developed mixed convection flow in various geometries, showing that the flow profiles may vary dramatically from the isothermal flow case even for moderate heating or cooling. It can be shown that the fully developed flow is the same as that for constant heat flux at the walls (Morton 1960), and this was studied by Sherwin (1968) and Maitra and Subba Raju (1975) for annular flows. It is important to note that fully developed flows only exist in these flows if it is assumed that all physical quantities, except the density, do not depend on the temperature (see, for example, Chato and Lawrence 1964). The effect of natural convection on the flow is governed by the Rayleigh number, Ra, and for sufficiently large values of $|Ra|$ recirculation regions are present. It can be shown that when the temperature decreases with height, "thermal runaway" occurs at critical values of Ra (Jones 1992; Morton 1960; Ostrach 1954), the first being $0(10^2)$ (Jones 1992). Reverse flow is exhibited adjacent to the duct walls for large enough values of Ra below this first critical value of Ra (Jones and Ingham, 1991; Jones 1992). Beckett (1980) and Rokerya and Iqbal (1971) investigated the effect of viscous dissipation on the flow, showing that the velocity does not become infinite, but is multiple-valued near the critical values of Ra and that increasing the viscous dissipation decreases the flow rate for a given pressure gradient. Conversely, when the temperature increases with height, the velocity remains finite for all values of Ra and reverse flow regions appear initially at the center of the duct (Jones and Ingham 1991; Jones 1992).

The choice of numerical approach used in modeling combined convection flows depends on whether the magnitudes of the streamwise diffusion terms are considered negligible or significant. The comparative magnitude of the streamwise diffusion terms with respect to the advection, inertia, and transverse diffusion terms is dependent on the magnitudes of the Reynolds number, Re, and the Péclet number, Pe. It can be shown (Ingham *et al.* 1988a and 1988b) that the streamwise diffusion terms are negligible for Re, $Pe \gg 1$, which is the situation considered in this paper. The resulting equations are of a parabolic nature and hence can be solved using finite-difference techniques to find the solution at successive streamwise locations. Parabolic methods have been used for problems where the wall temperature varies in the streamwise direction (Aung and Worku 1987; Jones and Ingham 1991), and by solving the corresponding elliptic equations it can be shown that the parabolic solution method produces a good approximation of the flow for $Re = 0(10^2)$. Hence it is reasonable to assume that the parabolic approach provides a

Address reprint requests to Professor Ingham at the Department of Applied Mathematical Studies, Leeds University, Leeds LS2 9JT, UK.

Received 5 February 1992; accepted 11 May 1992

suitable approximation of the flow in the cases under consideration.

In this study the problem is formulated in a similar manner to the work performed by Ingham *et al.* (1988a) in terms of a nondimensional streamfunction, vorticity, and temperature. There are no difficulties in extending the analysis when primitive variables are used and the choice of a streamfunction–vorticity formulation is just a preference of the authors. In general, the use of a streamfunction–vorticity formulation in two-dimensional (2-D) and axisymmetric flows avoids difficulties in conserving fluid and the use of a pressure-correction equation. The solution procedure that is used is of a marching type in which the direction of the marching may be varied and the governing parameters are the Prandtl number, Pr, and the Grashof number, Gr = Ra/Pr. For the simple case where the flow is always in the direction of the entrance velocity, the finite-difference equations are solved, from the duct entrance into the region of fully developed flow, using an implicit method. This basic marching method uses only information from the previous streamwise location together with the boundary conditions on the walls, and hence only an inlet condition is needed in the streamwise direction. Recirculation regions have been observed experimentally by Morton *et al.* (1989) for the case of a pipe with a constant wall temperature over a finite length of pipe. The finite-difference technique described above becomes numerically unstable a few streamwise steps into a reverse flow region, as a result of neglecting vital upstream information. Developing flows have been studied by a large number of authors, both for the constant wall temperature case (Aung *et al.* 1972; Aung and Worku 1986; Bodoia and Osterle 1962; Collins 1980; El-Shaarawi and Sarhan 1980; Habchi and Acharya 1986; Hashimoto *et al.* 1986; Sherwin and Wallis 1971; Sparrow *et al.* 1984) and for the constant heat flux case (Aung and Worku 1987; Penot and Dalbert 1983). None of these papers was able to obtain solutions for anything but very weak flow reversals. Cebeci *et al.* (1982) computed reverse flow solutions by solving the boundary-layer equations and using the approximation of Reyhner and Flügge-Lotz (1968), while Yao (1983) obtained an analytical solution near the entrance region of a channel for both the above cases, but did not deal with flow reversal. Ingham *et al.* (1988a) overcame the problem of numerical stability in reverse flows for the case where constant wall temperatures are applied, by using an iterative technique similar to that used by Williams (1975) for a boundary-layer flow.

No experimental data are available for developing mixed convection flows in pipes and ducts where the temperature on the walls vary linearly with height, even though this problem has numerous applications in the oil industry, e.g., the flow of muds and cements down oil wells during drilling and cementing. Because of this lack of experimental data on this problem, the aim of the present work is to develop a simple model for the developing mixed convection flow between vertical parallel plates where the temperature varies linearly with height, to describe a robust computational scheme, and to identify the parameter ranges in which various types of solutions are possible. In particular, the presence of reverse flows in the cementing process of oil wells causes the on-site engineer many problems. In order to be able to make any progress on this problem, some simplifying assumptions have to be made, in

Notation

d Half-width of the duct
f Friction factor
g Gravitational acceleration
Gr Grashof number, $g\beta\lambda d^3/\nu^2$
h Local heat transfer coefficient of the fluid
I First transverse point of forward flow
H Finite-difference step size across the duct
k Thermal conductivity of the fluid
K Finite-difference step size along the duct
m Streamwise location in the blending region
M Number of variables in iteration procedure, $(3N-1)(j_f+n-j_b+1)$
n Number of streamwise finite-difference steps in the blending region
N Number of finite-difference steps across the duct
NN Number of finite-difference steps along the duct
Nu Nusselt number, hd/k
P Point in Figure 2 at which the approximation predicts forward flow and the final solution predicts reverse flow
Pe Péclet number, RePr
Pr Prandtl number, ν/α
Ra Rayleigh number, GrPr
Re Reynolds number, dv_m/ν
T Temperature
u Transverse velocity component
U Dimensionless transverse velocity component, u/v_m
v Streamwise velocity component
V Dimensionless streamwise velocity component, v/v_m
W Width of the recirculation region
x Transverse coordinate
X Dimensionless transverse coordinate, x/d
y Streamwise coordinate
Y Dimensionless streamwise coordinate, $y/(d\mathrm{Re})$

Greek symbols

α Molecular thermal diffusivity of the fluid
β Coefficient of thermal expansivity of the fluid, $(-1/\rho_0)(\partial\rho/\partial T)$
δ Convergence parameter for the iteration process
ϵ Parameter for the doubling of the streamwise step length
ε Convergence parameter for the marching process
λ Temperature gradient applied to the walls
ν Kinematic viscosity of the fluid
ρ Density of the fluid
σ Characteristic difference between solutions at Y_f and as $Y \to \infty$
θ Dimensionless temperature, $(T-T_0)/(\mathrm{Re}\lambda) + y/(d\mathrm{Re})$
ψ Dimensionless streamfunction
Ω Dimensionless vorticity

Subscripts

b Value at the beginning of the reverse flow region
dev Development length
div Value at the transverse extreme of the reverse flow region
f Value at the end of the marching region
i Transverse finite-difference suffix
j Streamwise finite-difference suffix
m Flow average value
w Value at the wall

particular the following:

(1) All physical quantities except the density do not depend on the temperature. If this assumption is not made, then there is no fully developed flow solution (see Chato and Lawrence 1964). In some circumstances this may not be a good approximation; for example, Collins *et al.* (1977) found that for oils the variation with temperature of the viscosity was just as important as the density changes. However, Scheele and Hanratty (1962) stated that their "experiments indicated that changes in the flow field resulted primarily from natural convection effects rather than viscosity variations." Because no experimental data are available at the moment, and because we are interested here in the general trends rather than detailed predictions, this assumption appears to be reasonable.
(2) The wall temperatures are specified. In practice, heat flow in the walls of the channel will take place, and in the drilling of oil wells the linear variation of the temperature with depth from the surface will only be achieved at large distances from the position at which drilling takes place. Thus in general a heat-flux boundary condition should be applied, and this will involve a parameter that involves the thermal conductivities and heat transfer coefficients of the relevant materials. Therefore, in order to reduce the number of parameters involved in the problem, the wall temperatures are specified.
(3) The Prandtl number is unity. In practice, Prandtl numbers of fluids tend to be greater than unity; for the muds and cements that are used in drilling and cementing, the Prandtl number is typically $0(10^2)$. However, in order to compare the results with existing published works, a Prandtl number of unity has been taken.
(4) The fluid flow is stable. However, it has for a long time been known that these types of flows are prone to instabilities (see, for example, Barozzi *et al.* (1984) and Yao (1987)). Barozzi *et al.* (1984), and the references contained there, indicate that instabilities in the flow are possibly related to a minimum value of the local Nusselt occurring, although this is not entirely borne out by Morton *et al.* (1989). The study of instabilities occurring in this kind of flow is beyond the scope of this paper, since no experimental data are available to test any theoretical predictions.
(5) The flow is Newtonian. In practice, muds and cements are non-Newtonian fluids, and this effect is at present under investigation.

Since at the moment we are interested in general trends rather than detailed predictions, and since no experimental data are available, the number of parameters occurring has been reduced to a minimum, and all the above assumptions are reasonable.

Ingham *et al.* (1988b) attempted to solve situations akin to those studied in this paper, namely, mixed convection flows in a vertical duct with the temperature on the walls varying linearly with height. However, they neglected to set an upstream condition, using only the initial approximate boundary condition. Although this nonrigorous method gives surprisingly accurate results in the presented cases, it relies on the precision of the initial approximation and is therefore not considered adequate for use in the present case. In this paper, a fully developed boundary condition is used upstream in the recirculation region, and a blending region between this upstream boundary condition and the initial approximation is required to ensure the stability of the numerical scheme.

Complete solutions have been obtained for developing flows, including situations where flow separation occurs. The results that are achieved show good agreement with the analytical results obtained for the kinematically and thermally fully developed flow region (Jones 1992).

The model and governing equations

Consider the steady laminar convection flow of a Newtonian fluid between two vertical parallel plates at $x = \pm d, 0 \leqslant y < \infty$, where y is measured vertically downwards, as illustrated in Figure 1. It is assumed that the fluid flows through a constriction at $y = 0$ in a fashion that causes the velocity at $y = 0$ to be uniform. The velocity is given by $(0, v_m)$ at $y = 0$ and (u, v) for $y > 0$, the velocity components being in the x- and y-directions, respectively. The walls are maintained at a uniform temperature gradient, λ/d, so that the temperature on the walls, T_w, is given by $T_w = T_0 - \lambda y/d$, where T_0 is the temperature of the wall at the inlet, $y = 0$. The fluid and the walls are considered to have the same temperature at the inlet, so that the buoyancy effects are caused only by the presence of the temperature gradient.

All the physical properties of the fluid, except density, are assumed to be constant; the Boussinesq approximation is used, and viscous dissipation is neglected in the energy equation, since this can be shown to have only a small effect at the values of Ra considered here. However, viscous dissipation must be included for negative values of the Rayleigh number of $0(10^2)$ (Jones 1992). It is assumed that the temperature gradient is great enough for the effects of natural and forced convection to be of the same order of magnitude.

The governing equations are the continuity, transverse momentum, and energy equations; these can be simplified as shown by Jones and Ingham (1991) to the following non-dimensional form

$$\Omega = \frac{\partial^2 \psi}{\partial X^2} \tag{1}$$

$$\frac{\partial \psi}{\partial X}\frac{\partial \Omega}{\partial Y} - \frac{\partial \psi}{\partial Y}\frac{\partial \Omega}{\partial X} = \frac{\partial^2 \Omega}{\partial X^2} - \mathrm{Gr}\frac{\partial \theta}{\partial X} \tag{2}$$

$$\mathrm{Pr}\left(\frac{\partial \psi}{\partial X}\left(\frac{\partial \theta}{\partial Y} - 1\right) - \frac{\partial \psi}{\partial Y}\frac{\partial \theta}{\partial X}\right) = \frac{\partial^2 \theta}{\partial X^2} \tag{3}$$

The Prandtl number is given by $\mathrm{Pr} = \nu/\alpha$ and $\mathrm{Gr} = g\beta\lambda d^3/\nu^2$ is the Grashof number, where $\beta = (-1/\rho_0)(\partial\rho/\partial T)$ is the coefficient of thermal expansivity, ρ_0 is the density, α is the molecular thermal diffusivity of the fluid, and g is the gravitational acceleration.

The coordinates X, Y are nondimensional and are given by $x = dX$ and $y = \mathrm{Re}\, dY$, respectively. The scaling with respect to the Reynolds number in the vertical direction ensures that

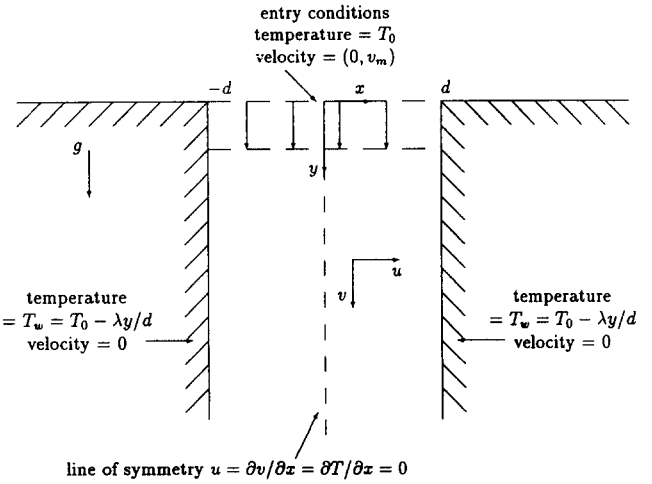

Figure 1 A schematic diagram of the flow geometry

the flow development lengths are $0(1)$ as $\mathrm{Re} \to \infty$. The nondimensional streamfunction, vorticity, and temperature—ψ, Ω, and θ, respectively—are defined as follows:

$$U = -\frac{1}{\mathrm{Re}}\frac{\partial \psi}{\partial Y}, \qquad V = \frac{\partial \psi}{\partial X} \tag{4}$$

$$\Omega = \frac{\partial V}{\partial X} - \frac{1}{\mathrm{Re}}\frac{\partial U}{\partial Y} \tag{5}$$

$$\theta = \frac{T - T_0}{\lambda\,\mathrm{Re}} + Y \tag{6}$$

where $\mathrm{Re} = v_m d/\nu$ is the Reynolds number, v_m is a characteristic velocity, taken to be the mean streamwise velocity in this study, and ν is the kinematic viscosity; U and V are the nondimensional velocities defined by

$$u = v_m U, \qquad v = v_m V \tag{7}$$

The simplification that is required in order to obtain the governing equations 1 to 3 relies on the fact that the streamwise diffusion terms are $0(1/\mathrm{Re}^2)$, so for $\mathrm{Re} \gg 1$ and $\mathrm{Pr} = 0(1)$ these terms can be neglected.

By utilizing the symmetry of the problem about $x = 0$, $0 \leqslant y < \infty$, the solution domain can be reduced to the half-duct, $0 \leqslant x \leqslant d$, $0 \leqslant y < \infty$, and the nondimensional boundary conditions are as follows:

$$\text{At } X = 0 \quad 0 \leqslant Y \leqslant \infty \qquad \begin{cases} \psi = 0, \quad \Omega = 0 \\ \dfrac{\partial \theta}{\partial X} = 0 \end{cases} \tag{8}$$

$$\text{At } X = 1 \quad 0 \leqslant Y < \infty \qquad \begin{cases} \psi = 1, \theta = 0 \\ \dfrac{\partial \psi}{\partial X} = 0 \end{cases} \tag{9}$$

$$\text{At } Y = 0 \quad 0 \leqslant X \leqslant 1 \qquad \psi = X, \quad \Omega = 0, \quad \theta = 0 \tag{10}$$

where ψ is arbitrarily set to zero on $X = 0$.

Hence, Equations 1 to 3 describe the flow and are solved subject to the boundary conditions 8 to 10.

The numerical scheme, including reverse flow situations

A finite-difference approach is used to solve the equations. The most appropriate scheme was found to be a fully implicit scheme with backward differencing in the streamwise direction and central differencing in the transverse direction. This is modified in the reverse flow regions.

Forward flow regions

Using the above scheme, the finite-difference forms of Equations 1 to 3 are

$$\Omega_{i,j+1} = \frac{1}{H^2}(\psi_{i+1,j+1} - 2\psi_{i,j+1} + \psi_{i-1,j+1}) \tag{11}$$

$$\begin{aligned} &\frac{1}{2HK}[(\psi_{i+1,j+1} - \psi_{i-1,j+1})(\Omega_{i,j+1} - \Omega_{i,j}) \\ &\quad - (\Omega_{i+1,j+1} - \Omega_{i-1,j+1})(\psi_{i,j+1} - \psi_{i,j})] \\ &= \frac{1}{H^2}(\Omega_{i+1,j+1} - 2\Omega_{i,j+1} + \Omega_{i-1,j+1}) \\ &\quad - \frac{\mathrm{Gr}}{2H}(\theta_{i+1,j+1} - \theta_{i-1,j+1}) \end{aligned} \tag{12}$$

$$\begin{aligned} &\frac{1}{2HK}[(\psi_{i+1,j+1} - \psi_{i-1,j+1})(\theta_{i,j+1} - \theta_{i,j}) \\ &\quad - (\theta_{i+1,j+1} - \theta_{i-1,j+1})(\psi_{i,j+1} - \psi_{i,j})] \\ &\quad - \frac{1}{2H}(\psi_{i+1,j+1} - \psi_{i-1,j+1}) \\ &= \frac{1}{\mathrm{Pr}H^2}(\theta_{i+1,j+1} - 2\theta_{i,j+1} + \theta_{i-1,j+1}) \end{aligned} \tag{13}$$

where the suffixes (i, j) refer to the point $X = (i-1)H$ on the jth streamwise locations and H, K are the constant transverse and variable streamwise step sizes, respectively. Defining the number of steps across the half-duct, $0 \leqslant X \leqslant 1$, to be N, sets $H = 1/N$. The number of streamwise steps, NN, is chosen so that the flow has converged to within a given tolerance of the fully developed flow, given by Jones (1992) as

$$V(X) = \frac{\mathrm{Ra}^{\dagger 1/4}}{\tan \mathrm{Ra}^{\dagger 1/4} - \tanh \mathrm{Ra}^{\dagger 1/4}} \times \left(\frac{\cos(\mathrm{Ra}^{\dagger 1/4}X)}{\cos \mathrm{Ra}^{\dagger 1/4}} - \frac{\cosh(\mathrm{Ra}^{\dagger 1/4}X)}{\cosh \mathrm{Ra}^{\dagger 1/4}}\right) \tag{14}$$

$$\theta(X) = \frac{1}{\mathrm{Ra}^{\dagger 1/4}(\tan \mathrm{Ra}^{\dagger 1/4} - \tanh \mathrm{Ra}^{\dagger 1/4})} \times \left(\frac{\cos(\mathrm{Ra}^{\dagger 1/4}X)}{\cos \mathrm{Ra}^{\dagger 1/4}} + \frac{\cosh(\mathrm{Ra}^{\dagger 1/4}X)}{\cosh \mathrm{Ra}^{\dagger 1/4}} - 2\right) \tag{15}$$

where $\mathrm{Ra}^{\dagger} = -\mathrm{Ra}$, so $\mathrm{Ra}^{\dagger 1/4}$ can take real or complex values. The values of Ra for which flow reversal first occurs in the fully developed flow can be deduced from Equation 14. Flow reversal near the wall initially occurs when $dV/dX|_{X=1} = 0$, i.e., $\mathrm{Ra} = -31.3$, while flow reversal at the center of the duct occurs first when $V|_{X=0} = 0$, i.e., $\mathrm{Ra} = 4\pi^4 = 389.6$. Hence, flow reversals occur for $\mathrm{Ra} > 389.6$ and $\mathrm{Ra} < -31.3$. However, at values of Ra above 6234.2 and below -913.9, the flow profiles have more than one recirculation region in the fully developed flow and are not considered here.

The boundary conditions 8 and 9 are

$$\psi_{1,j+1} = 0, \qquad \Omega_{1,j+1} = 0 \tag{16}$$

$$\psi_{N+1,j+1} = 0, \qquad \theta_{N+1,j+1} = 0 \tag{17}$$

and $\theta_{1,j}$ is evaluated using the Taylor expansion about $X = 0$. Hence, the expression

$$3\theta_{1,j+1} - 4\theta_{2,j+1} + \theta_{3,j+1} = 0 \tag{18}$$

is accurate to $0(H^4)$, and so the accuracy is consistent with the numerical scheme. Finally, $\Omega_{N+1,j+1}$ can be deduced from Equation 9 by using the Taylor expansion for Ω and ψ about $X = 1$ together with a backward difference equation for $\partial\Omega/\partial X$ at $X = 1$, leading to

$$\Omega_{N+1,j+1} = -\frac{3}{H^2}(1 - \psi_{N,j+1}) - \frac{1}{2}\Omega_{N,j+1} + 0(H^2) \tag{19}$$

Equations 11 to 13 and 16 to 19 define $3N - 1$ equations with $3N - 1$ unknowns and can be solved provided that the equations are linearized to provide an explicit form for the finite-difference variables at the $j + 1$th step. To do this, the transverse derivatives of ψ, θ, and Ω are evaluated at the jth step instead of the $j + 1$th step whenever they are multiplied by a streamwise derivative. Equations 11 to 13 and 16 to 19 then define a set of simultaneous linear equations in the finite-difference variables at the $j + 1$th step; Gaussian elimination may then be used to solve the problem at this streamwise step.

As the value of |Gr| increases, free convection effects increase and hence the kinematic and thermal development lengths increase. The scheme is modified to allow for the doubling of the streamwise step-size to ensure that the accuracy of the solution in the entry region is sufficient while reasonable computation times and storage requirements are maintained. At certain intervals, the solution at the $j+1$th streamwise location is recalculated with a step-size of $2K$. In practice, this need only be repeated at most once every five steps. The step-length is doubled if the following criterion is satisfied:

$$\frac{1}{3N-1}\sqrt{\sum_i [(\psi^K_{i,j+1}-\psi^{2K}_{i,j+1})^2+(\Omega^K_{i,j+1}-\Omega^{2K}_{i,j+1})^2 + \sqrt{(\theta^K_{i,j+1}-\theta^{2K}_{i,j+1})^2}]} < \varepsilon \quad (20)$$

where the superscripts refer to the step-size with which the variables were calculated, and ε is usually taken to be about 10^{-3}. This adaptation to the technique drastically increases the step-size towards the fully developed region.

Reverse flow regions

Reverse flow regions appear, either near the wall or at the center of the duct, as the value of |Gr| increases. At still larger values of |Gr|, the flow profiles become more complex, with more recirculation regions; these can be dealt with in a similar fashion to the work in this study, but are not considered here. The method described in the previous section becomes unstable after only a few steps into the reverse flow regions and so must be adapted. The first stage in the modification is to construct an approximation to the solution of the governing finite-difference equations, subject to the given boundary conditions. The approximation ensures that information only travels in the direction of the flow by replacing negative velocities with zero velocities in the evaluation of the next streamwise step. This is analogous to replacing the streamfunction by a monotonic increasing function with $0 \leqslant \psi_{i,j} \leqslant 1$ and $\psi_{i+1,j} \geqslant \psi_{i,j}$, for all $i = 1, \ldots, N$. After the evaluation of the variables at this step the original values of the streamfunction are replaced at the previous step. The approximation is obtained for $0 \leqslant X \leqslant 1$ and from the start of the reverse flow region, $Y = Y_b$, to a location, $Y = Y_f$, where the approximation has converged, within a given tolerance, to an approximate solution. This tolerance criterion is given by

$$\frac{1}{3N-1}\sqrt{\sum_{i=1}^{N+1} [(\psi_{i,j_f}-\psi_{i,j_f-1})^2+(\Omega_{i,j_f}-\Omega_{i,j_f-1})^2 + \sqrt{(\theta_{i,j_f}-\theta_{i,j_f-1})^2}]} < \varepsilon \quad (21)$$

where j_f corresponds to the streamwise location Y_f and the finite-difference variables are obtained using the approximation procedure. The value of ε is usually taken to be $0(10^{-5})$. It is assumed that over the distance Y_f the development lengths are sufficiently large to ensure that the final solution at Y_f is within some tolerance of the fully developed solution. This can be checked once the solution procedure has converged and the value of ε is decreased if Equation 21 is not satisfied.

To ensure that the correct information is swept downstream in the iteration procedure, a far-stream condition must be set in the recirculation region. This condition is chosen to be the fully developed flow and buoyancy profiles, which are given analytically by Equations 14 and 15, and is set at a streamwise position given by $j = j_f + n$. However, to ensure the stability of the method, the far-stream boundary condition must be consistent with the numerical scheme. Hence, using the analytical solution as an initial estimate, the solution to the finite-difference problem is found by iterating on Equation 11 and using the boundary conditions (Equations 16 to 19), with $j = j_f + n$, together with the following equations for $i = 2, \ldots, N$:

$$\Omega^{*s+1}_i = \frac{1}{2 \pm \frac{H}{2K}(\psi^{*s}_{i+1}-\psi^{*s}_{i-1})} \times \left(\Omega^{*s}_{i+1}+\Omega^{*s}_{i-1}-\frac{GrH}{2}(\theta^{*s}_{i+1}-\theta^{*s}_{i-1}) \pm \frac{H}{2K}\Omega^{*s}_i(\psi^{*s}_{i+1}-\psi^{*s}_{i-1})\right) \quad (22)$$

$$\theta^{*s+1}_i = \frac{1}{2 \pm \frac{PrH}{2K}(\psi^{*s}_{i+1}-\psi^{*s}_{i-1})} \times \left(\theta^{*s}_{i+1}+\theta^{*s}_{i-1}+\frac{PrH}{2}(\psi^{*s}_{i+1}-\psi^{*s}_{i-1}) \pm \frac{PrH}{2K}\theta^{*s}_i(\psi^{*s}_{i+1}-\psi^{*s}_{i-1})\right) \quad (23)$$

where the positive sign is taken if there is forward flow at the grid point i (i.e., $\psi^{*s}_{i-1} < \psi^{*s}_{i+1}$) and the negative sign is taken if there is reverse flow at the grid point i (i.e., $\psi^{*s}_{i-1} > \psi^{*s}_{i+1}$). The asterisk (*) denotes the finite-difference variable for the fully-developed flow. This pointwise approach is consistent with the iteration procedure that is used in the next step of the solution method and is preferred to a Gaussian elimination approach for reasons considered later.

There may be points where the solution obtained by the approximation at Y_f predicts forward flow and the fully developed solution predicts reverse flow. As shown in Figure 2, for the case $N = 10$, if the fully developed solution is imposed on the streamwise location Y_f, then the information at the point in the region P is never included in the solution, since the direction of the marching is determined by the flow at the points on the previous streamwise location. In this paper, N is taken to be 40, and so the number of points in the region P is greater than that shown. In the diagram the dotted lines represent the flow as determined by the approximation, while the unbroken lines represent the flow in the more accurate solution. The nature of the approximation causes insufficient flow to travel downstream, and hence the approximate recirculation regions are always narrower than the actual recirculation regions.

This problem is overcome by using a blending region between the final streamwise location obtained by the approximation Y_f and the fully developed solution. It may appear that more accurate solutions would be obtained by using a region scaled to infinity. However, since Equations 1 to 3 only possess single derivatives in the streamwise direction, convergence by this method is extremely slow. Hence, in this study, the blending function is defined by

$$A_{i,j_f+m} = A^*_i + (A_{i,j_f}-A^*_i)\left(1-\frac{m}{n}\right)^2 \quad \text{for } 0 \leqslant m \leqslant n \quad (24)$$

where A is each of the variables ψ, Ω, and θ in turn, and n is the number of added streamwise steps in the blending region. Hence, A_{i,j_f+n} is the fully developed solution, A^*_i, and A_{i,j_f} is the value of the variable obtained by the initial approximation at $Y = Y_f$. The blending function is a parabola in Y, with a turning point, and hence a minimum rate of change, at the final streamwise location corresponding to $j = j_f + n$. This is exactly what is required in the final solution, where the streamwise derivatives of the variables decrease with the value of Y.

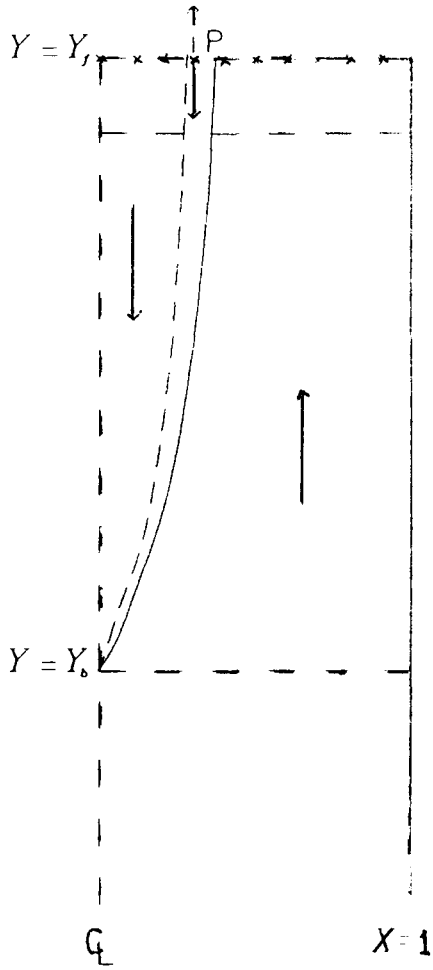

Figure 2 A schematic diagram showing the initial approximation and the final solution

The number of extra streamwise locations, n, is chosen so that the changes in the streamwise derivatives across $Y = Y_f$ are consistent with the corresponding changes at the previous streamwise location. This is achieved in the following manner. The difference between the solution at $Y = Y_f$ and the fully developed solution is characterized by σ where

$$\frac{1}{3N-1}\sqrt{\sum_{i=1}^{N+1}[(\psi_i^* - \psi_{i,j_f})^2 + (\Omega_i^* - \Omega_{i,j_f})^2 + \sqrt{(\theta_i^* - \theta_{i,j_f})^2}]} = \sigma \quad (25)$$

If the value of ε is taken to be $0(10^{-5})$, then the value of σ is usually $0(10^{-6})$. The root mean square error between the solution at adjacent streamwise locations is defined, on convergence, by ε in Equation 21. Now, by substituting $m = 1$ into Equation 24, an equation is obtained relating n to the appropriate errors at each transverse location

$$\frac{A_{i,j_f+1} - A_{i,j_f}}{A_{i,j_f} - A_i^*} = -\frac{2}{n} + \frac{1}{n^2} \quad (26)$$

and so for consistency n is chosen to satisfy

$$n = 0\left(\frac{\sigma}{\varepsilon}\right) \quad (27)$$

Although the variables themselves are approximately correct in the blending region, the derivatives of the variables are not as accurate. Hence, increasing the number of streamwise points in the blending region increases the size of the region for which the initial estimate is not as accurate as the initial approximation. Consequently, a moderate value of n that satisfies Equation 27 is chosen. In this study, n is taken to be between 20 and 50.

The next step of the solution procedure is to construct the finite-difference equations depending on the direction of the flow at a given point. These equations are then iterated upon, using the previous approximation as an initial estimate to the solution, until convergence is achieved. The equations are dealt with in a pointwise manner so that the relatively large inaccuracies in the reverse flow region and near the wall are not swept throughout the flow. This method for dealing with the iteration problem alters the values of the variables far less radically at each sweep than a Gaussian elimination method would, and hence the pointwise method is more stable than the matrix method. To explain the method in more detail, the situation of reverse flow at the center of the duct is investigated.

A downstream sweep is made in the region of reverse flow in $Y_b \leqslant Y \leqslant Y_f$, using information from the previous upstream location, i.e., using forward differencing. Equations 11 to 13 are not linearized, since the nonlinear terms can be replaced by their values at the previous iteration, hence the pointwise equations are given by

$$\psi_{i,j}^{s+1} = \frac{1}{2}(\psi_{i+1,j}^s + \psi_{i-1,j}^s) - \frac{H^2}{2}\Omega_{i,j}^s \quad (28)$$

$$\Omega_{i,j}^{s+1} = \frac{1}{2 + \frac{H}{2K}(\psi_{i+1,j}^s - \psi_{i-1,j}^s)} \times \left(\Omega_{i+1,j}^s + \Omega_{i-1,j}^s - \frac{\mathrm{Gr}H}{2}(\theta_{i+1,j}^s - \theta_{i-1,j}^s) - \frac{H}{2K}(\psi_{i+1,j}^s - \psi_{i-1,j}^s)\Omega_{i,j+1}^s + \frac{H}{2K}(\Omega_{i+1,j}^s - \Omega_{i-1,j}^s)(\psi_{i,j+1}^s - \psi_{i,j}^s)\right) \quad (29)$$

$$\theta_{i,j}^{s+1} = \frac{1}{2 + \frac{\mathrm{Pr}H}{2K}(\psi_{i+1,j}^s - \psi_{i-1,j}^s)} \times \left(\theta_{i+1,j}^s + \theta_{i-1,j}^s - \frac{\mathrm{Pr}H}{2}(\psi_{i+1,j}^s - \psi_{i-1,j}^s) - \frac{\mathrm{Pr}H}{2K}(\psi_{i+1,j}^s - \psi_{i-1,j}^s)\theta_{i,j+1}^s + \frac{H}{2K}(\theta_{i+1,j}^s - \theta_{i-1,j}^s)(\psi_{i,j+1}^s - \psi_{i,j}^s)\right) \quad (30)$$

The boundary conditions consist of the conditions at $X = 0$, given by Equations 16 and 18, together with the values of the variables at the first point of the forward flow region. If $X = HI$ is the first point at any particular streamwise location at which forward flow occurs, i.e., for all $i \geqslant I$, $\psi_{i+1,j} > \psi_{i-1,j}$ and for all $i < I$, $\psi_{i+1,j} \leqslant \psi_{i-1,j}$, then the boundary conditions for the

downstream sweep are given by

$$\psi_{I,j} = \psi^u_{I,j}, \qquad \Omega_{I,j} = \Omega^u_{I,j}, \qquad \theta_{I,j} = \theta^u_{I,j} \tag{31}$$

where u refers to the values calculated at the previous upstream sweep.

Similarly, in the upstream sweep the equations are obtained using backward differencing. They are solved in the forward flow region using the boundary conditions at $X = 1$, given by Equations 17 and 19, and the values of the variables at the last point of the reverse flow region that were calculated at the previous downstream sweep, i.e.,

$$\psi_{I-1,j} = \psi^d_{I-1,j}, \qquad \Omega_{I-1,j} = \Omega^d_{I-1,j}, \qquad \theta_{I-1,j} = \theta^d_{I-1,j} \tag{32}$$

where d refers to the values calculated at the previous downstream sweep.

Convergence is assumed to be achieved if

$$\frac{1}{M}\sqrt{\sum_{i=1}^{N+1}\sum_{j=j_b}^{j_f+n}\left[(\psi^{s+1}_{i,j} - \psi^s_{i,j})^2 + (\Omega^{s+1}_{i,j} - \Omega^s_{i,j})^2 + \sqrt{(\theta^{s+1}_{i,j} - \theta^s_{i,j})^2}\right]} < \delta \tag{33}$$

where s refers to the sth iteration, with one iteration consisting of an upward and downward sweep. The total number of variables in the iteration procedure M is given by

$$M = (3N - 1)(j_f + n - j_b + 1) \tag{34}$$

where j_b corresponds to the streamwise location Y_b. The iterative procedure is repeated until convergence is achieved, where δ is usually taken to be about 10^{-7}. This method allows for the gradual alteration of the position of the reverse flow region that is required for stability of the numerical scheme, whereas it was found that a Gaussian elimination method, together with S.O.R. techniques, did not converge. The pointwise method is far more robust than a full matrix method (Jones and Ingham 1991) and is necessary in order to ensure that the upstream boundary condition is slowly incorporated into the solution.

Reverse flows adjacent to the duct wall are dealt with in a similar manner and are therefore not described here.

Results

The results presented in this paper are calculated using a finite-difference grid with 40 uniform steps across the duct and between 40 and 400 steps of variable length along the duct. A numerical comparison between these results and those obtained using half the step-size across the duct would suggest that the solutions for ψ that are obtained using $N = 40$ are accurate to within 0.1 percent at each nodal point, with the greatest inaccuracies occurring near the entrance of the duct. The initial streamwise step length used in the calculation is 2.5×10^{-4}. The numerical scheme becomes unstable if this step-size is reduced below 1.0×10^{-4}, and this can only be overcome by decreasing the transverse step-size.

The character of the solutions depends on whether the free convection effects aid or oppose the forced convection effects, distinguished by whether the temperature increases or decreases with height (i.e., $Gr < 0$ and $Gr > 0$, respectively). This differs from the constant wall temperature case (Ingham *et al.* 1988a, 1988b), where the solution character depends on a combination of the change in temperature at the inlet and the direction of the streamwise velocity (i.e., Gr/Re). In the linear wall temperature case, the solution is independent of the direction of the mean flow and depends only on the orientation and strength of the temperature gradient.

The results in this paper are obtained using a value of unity for the Prandtl number, Pr, in order to compare the results to previously published work. However, a few test calculations have been performed for $10^{-2} \leqslant Pr \leqslant 10^2$, and the numerical technique worked efficiently in all cases. The results obtained for the upstream flow can be compared to the fully developed velocity and buoyancy profiles given in Equations 14 and 15.

For the smaller recirculation regions shown here, e.g., $Gr = -50$, the number of iterations that are required for convergence is generally between 400 and 600, while for the larger recirculation regions, e.g., $Gr = -75$, this may increase to 1,000 for the same level of convergence.

The results are presented in a manner that indicates the effect of varying the governing parameter, Gr. In Figure 3, velocity profiles are shown for $Gr = 0, -25, -50$, and -75 at the streamwise locations given by $Y = 0.0, 0.26, 0.51, 1.02$ and 1.47. The forced convection case corresponding to $Gr = 0$ is shown for comparison with the effect of buoyancy-aided flow ($Gr < 0$). These values of Y are indicative of the change in the velocity profiles as the fluid progresses along the duct. By $Y = 1.47$, the velocity profiles for the values of Gr shown in Figure 3 are graphically indistinguishable from the fully developed profiles in Equation 14. It can be seen that the free convection effects accelerate the streamwise velocity near the center of the duct, thus causing the velocity near the walls to decrease. As the value of Gr decreases, these effects become more marked, which eventually leads to separated flow at the wall for sufficiently large negative values of Gr.

Figure 4 presents the case where natural convection opposes the pressure force, i.e., $Gr > 0$, and velocity profiles are plotted for $Gr = 0, 300, 450$, and 600 at similar points along the duct to those shown in Figure 3. It can be seen that the effect of natural convection is to decelerate the flow around the center of the duct. The effects increase with the strength of the buoyancy force with respect to the viscous forces (i.e., increasing Gr). By $Gr = 450$, the effects are significant enough to cause recirculation at the center of the duct.

There are no reverse flow regions in the fully developed flow for $-31.3 < Gr < 389.6$. At values of Gr outside this range, the flow separates and the recirculation regions become more extreme as the value of $|Gr|$ increases. For $Gr < -913.9$ and $Gr > 6234.2$, more than one recirculation region exists in the fully developed flow.

The flow average temperature is defined at any particular streamwise location by Shah and London (1978):

$$T_m = \frac{1}{dv_m}\int_0^d vT\,dx \tag{35}$$

Hence, writing T and v in terms of ψ and θ, the flow average temperature can be described by

$$\theta_m = \int_0^1 \frac{\partial\psi}{\partial X}\theta\,dX \tag{36}$$

This integral can then be evaluated using Simpson's rule, and its value is plotted as a function of Y in Figure 5a for the values of Gr considered previously. It can be clearly seen that the flow average temperature at any given streamwise location decreases with increasing values of Gr, implying that heat transfer by convection takes place more efficiently when free convection effects oppose the forced convection effects. As $Y \to \infty$, the value of θ_m increases towards the fully developed value (Jones 1992), at $Y = 4$ it is within 10^{-2} of this value, while at $Y = 10$ the difference in the two values is less than 10^{-3}, corresponding to less than 0.2 percent error.

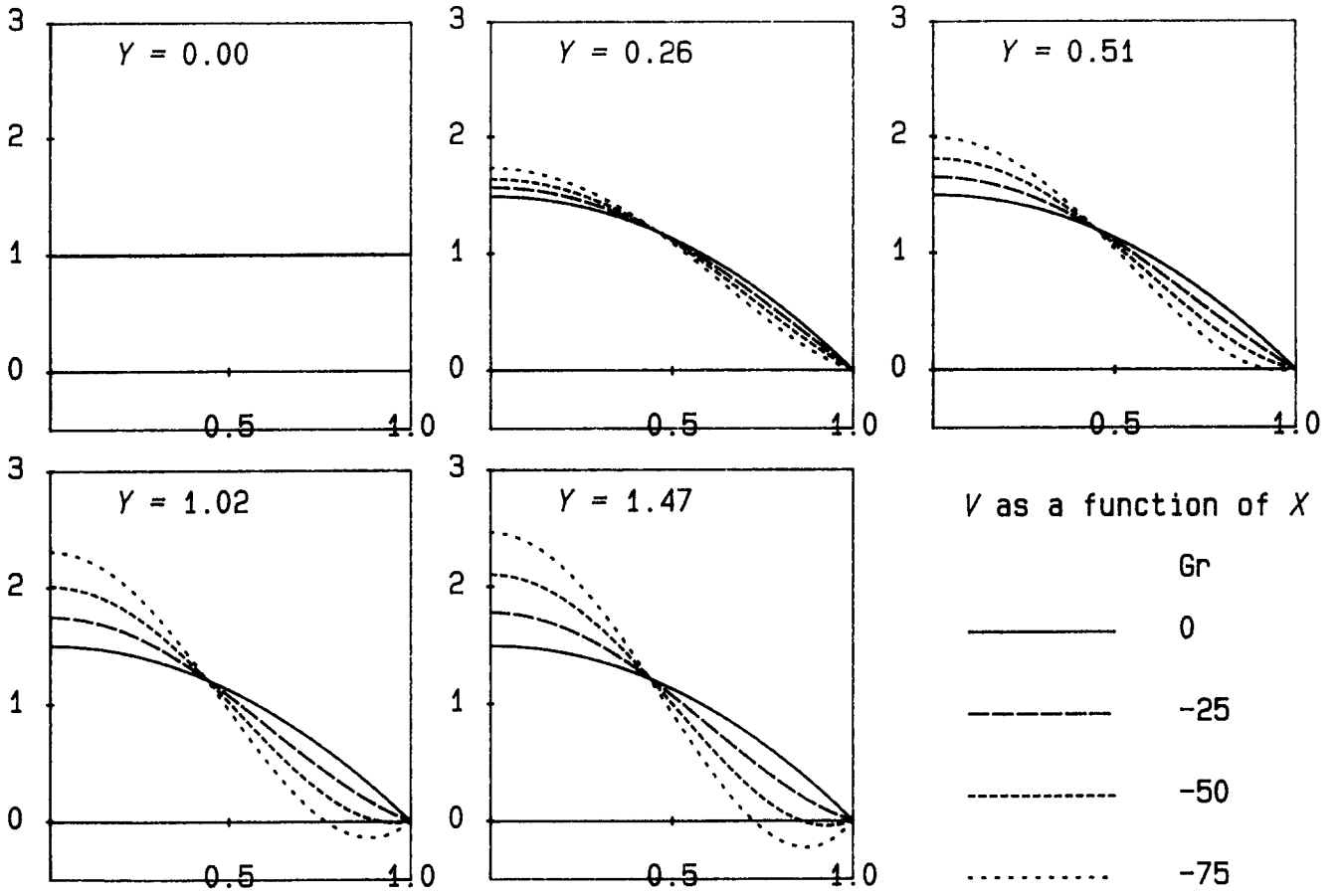

Figure 3 The velocity profiles for Gr = −75, −50, −25, and 0 at various streamwise locations

Applying Newton's law of cooling at the wall, namely,

$$h(T_m - T_w) = -k \left.\frac{\partial T}{\partial x}\right|_{x=d} \tag{37}$$

and defining the local Nusselt number by $\mathrm{Nu} = hd/k$, where h is the local heat transfer coefficient and k is the thermal conductivity of the fluid, leads to

$$\mathrm{Nu} = -\frac{\left.\frac{\partial \theta}{\partial X}\right|_{X=1}}{\theta_m} \tag{38}$$

Figure 5b displays plots of Nu as a function of Y for the same parameters as in Figure 5a. It can be seen that the value of Nu is large for large positive values of Gr, again implying that the heat transfer is more efficient in flows where the free convection effects oppose the forced convection effects. The behavior of Nu as a function of Y is characterized by the sign of Gr. For Gr > 0 there is an initial decrease in the value of Nu as the value of Y increases, and this is followed by an increase in the value of Nu. Thus a minimum value of Nu exists. Barozzi *et al.* (1984), as well as some of the references cited in this paper, suggest that in these circumstances instabilities may occur in the flow, and hence steady recirculating flows may not exist near the center of the duct. As explained earlier, the stability of these flows is beyond the scope of this paper, and conclusions about the stability of these flows at moment can only be speculative. As the value of Gr increases, the streamwise location at which the minimum Nusselt number occurs tends towards the duct entrance. Hence, the streamwise location at which heat transfer by convection is least efficient is near the duct entrance. For Gr < 0 there is a steady decrease in the value of the Nusselt number, and hence the heat transfer, along the duct.

For both Gr < 0 and Gr > 0, the value of Nu tends towards the fully developed value defined by

$$\mathrm{Nu} = \frac{1}{\theta_m} \tag{39}$$

as $Y \to \infty$. At $Y = 4$, the Nusselt number is within 10^{-2} of the fully developed value, and at $Y = 10$, it is within 10^{-3} of this value (i.e., less than 0.3 percent error).

The friction factor, f, is a measure of the frictional pressure drop in the system and is defined at any streamwise location by Özişik (1985) as follows:

$$f = -\frac{8\nu}{v_m^2} \left.\frac{\partial v}{\partial x}\right|_{x=d} \tag{40}$$

Substituting $v = v_m V$, $V = \partial\psi/\partial X$, and $x = dX$, and using Equation 1, Equation 40 becomes

$$f = -\frac{8}{\mathrm{Re}} \Omega|_{X=1} \tag{41}$$

Figure 5c shows the variation in Re f for the cases outlined for Figures 5a and 5b. For Gr < 0 (Gr > 0), the friction factor times Reynolds number is less (greater) than for the forced convection case. The friction factor itself depends on the Reynolds number, so for flows in the opposite direction to those indicated in Figure 1, i.e., Re < 0, the friction factor has the

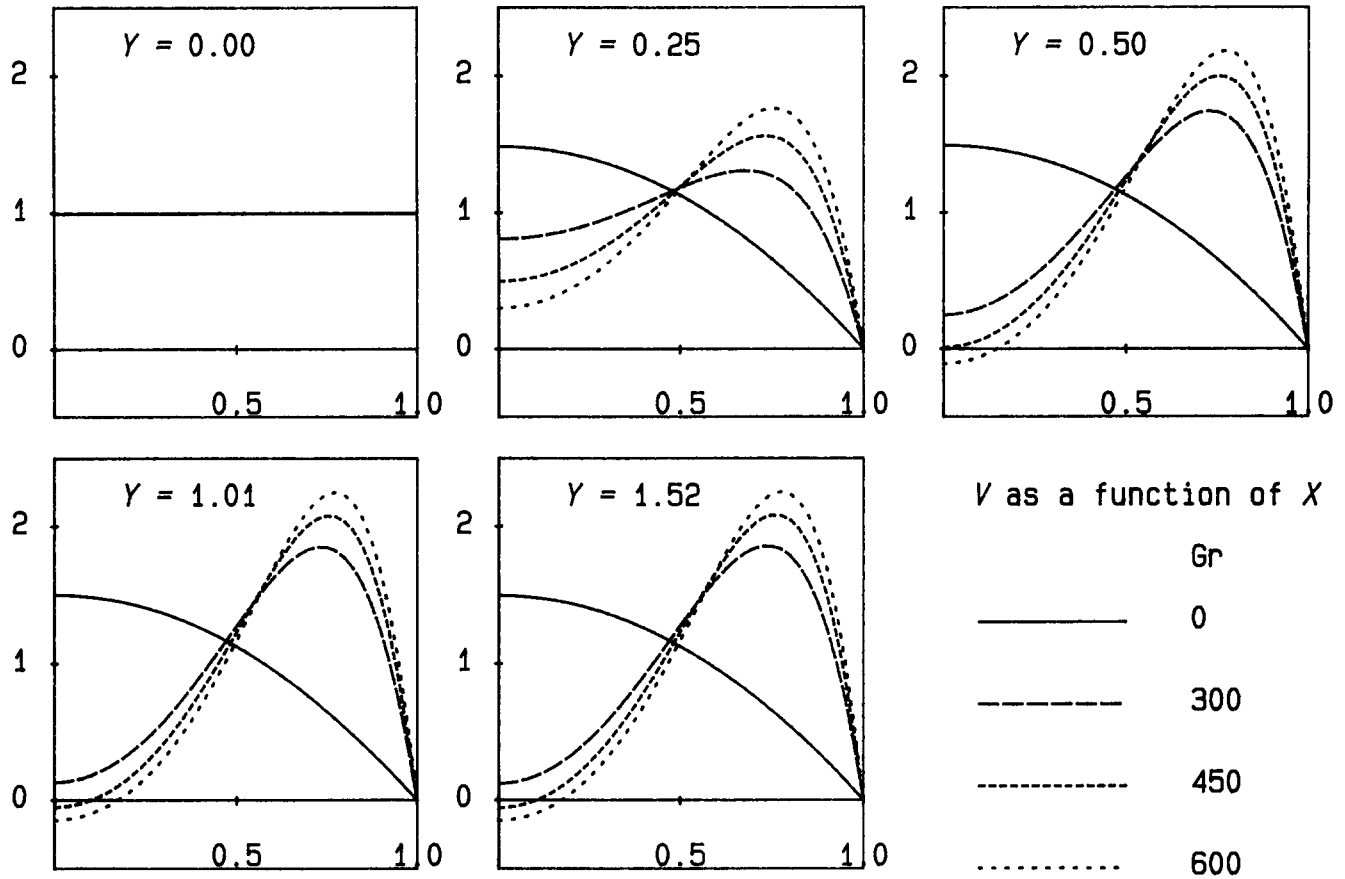

Figure 4 The velocity profiles for Gr = 0, 300, 450, and 600 at various streamwise locations

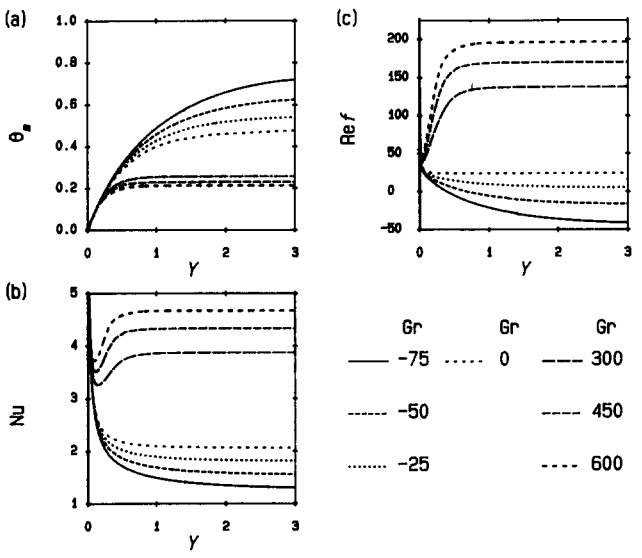

Figure 5 The development along the duct of (a) the mean buoyancy, (b) the local Nusselt number, and (c) the Reynolds number times friction factor for Gr = −75, −50, −25, 0, 300, 450, and 600

opposite sign to those shown here. For a given value of Re > 0, the friction factor is large and positive when the centerline velocity is at a minimum and hence the streamwise velocity peak near the duct wall is at a maximum.

The strength and position of the recirculation regions are characterized by the width of the fully developed flow region and the streamwise location at which reverse flow first occurs, respectively. In the fully developed flow, the transverse point, $X = X_{div}$, at the extreme of the reverse flow region is given by

$$\cos(\mathrm{Ra}^{\dagger 1/4} X_{div}) = \cosh(\mathrm{Ra}^{\dagger 1/4} X_{div}) \quad (42)$$

For $-389.6 < \mathrm{Ra}^{\dagger} < 31.3$, i.e., $-31.3 < \mathrm{Ra} < 389.6$, Equation 42 has no solutions in the range $0 < X_{div} \leqslant 1$. However, for $\mathrm{Ra}^{\dagger} > 31.3$, i.e., $\mathrm{Ra} < -31.3$, the width of the recirculation region in $0 \leqslant X \leqslant 1$ is given by $W = 1 - X_{div}$, while for $\mathrm{Ra}^{\dagger} < -389.6$, i.e., $\mathrm{Ra} > 389.6$, it is given by $W = X_{div}$. Figure 6 shows W as a function of Gr, where $\mathrm{Gr} = \mathrm{Ra} = -\mathrm{Ra}^{\dagger}$ if $\mathrm{Pr} = 1$. It can be seen that W increases more rapidly for Gr < 0 than for Gr > 0; even for Gr = 1,000, the recirculation region still occupies less than 1/5 of the width of the duct, while for Gr = 100 the recirculation regions occupy almost half the width of the duct. However, it is interesting to note that for these values of Gr the actual widths of the recirculation regions in $-1 \leqslant X \leqslant 1$ are approximately equal. For Gr < 0 there are two recirculation regions adjacent to the duct walls, while for Gr > 0 there is one central recirculation region. Thus, the actual width of each recirculation region is given by W for Gr < 0 and $2W$ for Gr > 0. As the value of |Gr| increases, there is a steady increase in the value of W for Gr < 0. However, for Gr > 0 the value of W increases rapidly as the value of |Gr| increases, until Gr is approximately 500. The increase in the value of W is then more gradual for $500 \leqslant \mathrm{Gr} \leqslant 1000$.

Figure 7 shows the streamwise location, Y_b, at which separation of the flow first occurs as a function of Gr. The value of Y_b decreases as the value of |Gr| increases (taking Y_b to be infinite for values of Gr in the range $-31.3 < \mathrm{Gr} < 389.6$). There is a rapid decrease in Y_b for $389.6 < \mathrm{Gr} < 500$,

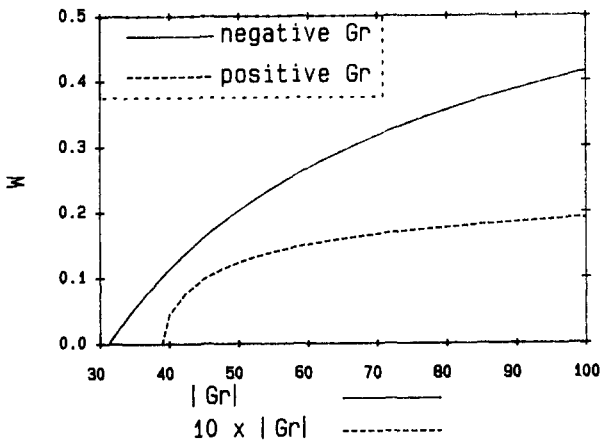

Figure 6 The width of the reverse flow regions in the fully developed flow, W, as a function of the Grashof number, Gr

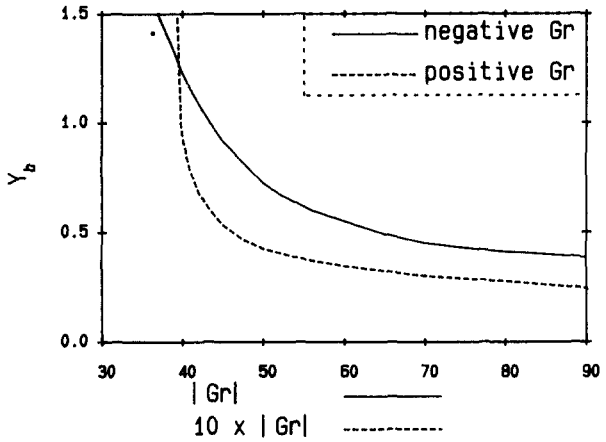

Figure 7 The streamwise location, Y_b, at which separation first occurs, as a function of the Grashof number, Gr

whereas the decrease in Y_b for $-50 < Gr < -31.3$ is steadier. By studying the corresponding value of Y_b for various actual duct widths (i.e., W for $Gr < 0$ and $2W$ for $Gr > 0$), it can be seen that when the widths of the recirculation regions in the fully developed flow are the same, then separation occurs nearer to the duct entrance for $Gr > 0$ than for $Gr < 0$. This is due to the increased heat transfer characteristics of $Gr > 0$ compared with $Gr < 0$, implying that the flows develop more quickly for $Gr > 0$.

Since the value of the Nusselt number depends on both the velocity and temperature distributions at any given streamwise location, an efficient assessment of when the flow becomes thermally and kinematically fully developed is when the Nusselt number is sufficiently close to its fully developed value. In this study this tolerance value is chosen to be 95 percent of the fully developed value. Figure 8 shows the corresponding development lengths as a function of Gr. By using a Levenberg–Marquardt method (Press *et al.* 1986) to fit a nonlinear curve through these data points, it is found that the development lengths are given approximately by

$$y_{dev} \simeq \left(0.722 \left(\frac{\left(1 - \tanh \frac{Gr}{1000}\right)^{7.92}}{\left(1 + \tanh \frac{Gr}{1000}\right)^{6.23}} \right) Re \right) d \qquad (43)$$

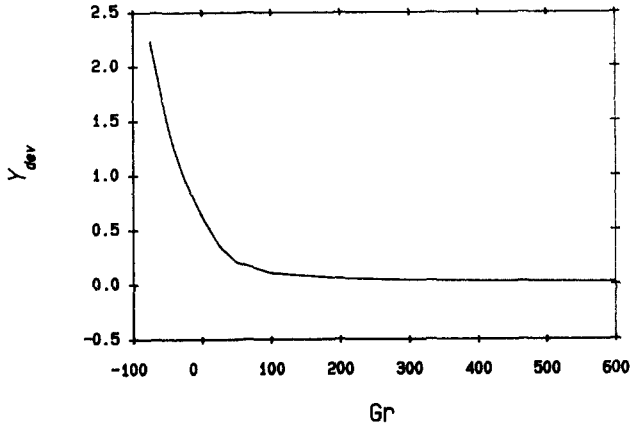

Figure 8 The velocity development lengths, Y_{dev}, as a function of the Grashof number, Gr

Over the range of values of Gr and Re given by $-75 \leqslant Gr \leqslant 600$ and $Re \gg 1$, Equation 43 generates values for y_{dev} that are accurate to within 10^{-2} of the results obtained from the parabolic solution.

Conclusion

In this paper, numerical solutions are obtained using parabolic methods for solving mixed convection flows in vertical parallel-plate ducts with linearly varying wall temperatures. Attention is concentrated on situations where the effects of free convection are large enough to cause recirculating flow near the center of the duct or adjacent to the duct walls. Situations where the fully developed flow profiles include regions of reverse flow are dealt with using an iterative technique, and a suitable approximation is suggested as an initial estimate. Some adaptations to ensure the stability of the numerical scheme are described.

It is shown that heat transfer by convection increases as a function of the Grashof number, Gr, and that development lengths decrease as the value of Gr increases. This agrees with the expected conclusion that heat transfer is improved if the free convection aids the forced convection adjacent to the walls. A correlation is given for the development lengths when the Prandtl number has a unitary value.

The techniques presented in this paper may be extended to non-Newtonian fluids and other geometries, in particular, cylindrical geometries such as pipes and annuli.

Acknowledgment

The authors would like to thank S.E.R.C. and Schlumberger Cambridge Research for their financial support of this work and also S. H. Bittleston for numerous constructive discussions.

References

Aung, W., Fletcher, L. S. and Sernas, V. 1972. Developing laminar free convection between vertical flat plates with asymmetric heating. *Int. J. Heat Mass Transfer*, **15**, 2293–2308

Aung, W. and Worku, G. 1986. Developing flow and flow reversal in a vertical channel with asymmetric wall temperatures. *ASME J. Heat Transfer*, **108**, 229–304

Aung, W. and Worku, G. 1987. Mixed convection in ducts with asymmetric wall heat fluxes. *ASME J. Heat Transfer*, **109**, 945–951

Barozzi, G. S., Dumas, A. and Collins, M. W. 1984. Sharp entry and

transition effects for laminar combined convection of water in vertical tubes. *Int. J. Heat Fluid Flow*, **5**, 235–241

Beckett, P. M. 1980. Combined natural and forced convection between vertical walls. *SIAM J. Appl. Math.*, **39** (2), 372–384

Bodoia, J. R. and Osterle, J. F. 1962. The development of free convection between heated vertical plates. *ASME J. Heat Transfer*, **84**, 40–54

Cebeci, T., Khattab, A. and Lamont, R. 1982. Combined natural and forced convection in vertical ducts. *Heat Transfer 1982, Proc. 7th Int. Heat Transfer Conf.* Munich, W. Germany, **3**, 419–424

Chato, J. C. and Lawrence, W. T. 1964. Chapter 14 in *Developments in Heat Transfer*, W. M. Rohsenow (ed.). Arnold, London

Collins, M. W. 1980. Finite difference analysis for developing laminar flow in circular tubes applied to forced and combined convection. *Int. J. Numer. Methods Eng.*, **15**, 381–404

Collins, M. W., Allen, P. H. G. and Szpiro, O. 1977. Computational methods for entry length heat transfer by combined convection in vertical tubes. *Proc. Inst. Mech. Eng.*, **191**, 19–29

El-Shaarawi, M. A. I. and Sarhan, A. 1980. Free convection effects on developing laminar flow in vertical concentric annuli. *ASME J. Heat Transfer*, **102**, 617–622

Habchi, S. and Acharya, S. 1986. Laminar mixed convection in a symmetrically or asymmetrically heated vertical channel. *Numer. Heat Transfer*, **9**, 605–618

Hashimoto, K., Akino, N. and Kawamura, H. 1986. Combined forced-free laminar heat transfer to a highly heated gas in a vertical annulus. *Int. J. Heat Mass Transfer*, **29**, 145–151

Ingham, D. B., Keen, D. J. and Heggs, P. J. 1988a. Two-dimensional combined convection in vertical parallel-plate ducts, including situations of flow reversal. *Int. J. Numer. Methods Eng.*, **26**, 1645–1664

Ingham, D. B., Keen, D. J. and Heggs, P. J. 1988b. Flows in vertical channels with asymmetric wall temperatures and including situations where reverse flows occur. *ASME J. Heat Transfer*, **110**, 910–917

Jones, A. T. and Ingham, D. B. 1991. Mixed convection flow of a Newtonian fluid in a vertical duct. *Proc. 1st I.C.H.M.T. Int. Numer. Heat Transfer Conf. Software Show*, Guildford, UK, 45–54

Jones, A. T. 1992. Combined convection in vertical ducts. Ph.D. Thesis, Department of Applied Mathematical Studies, Leeds University, Leeds, UK

Maitra, D. and Subba Raju, K. 1975. Combined free and forced convection laminar heat transfer in a vertical annulus. *ASME J. Heat Transfer*, **97**, 135–137

Morton, B. R. 1960. Laminar convection in uniformly heated vertical pipes. *J. Fluid Mech.*, **8**, 227–240

Morton, B. R., Ingham, D. B., Keen, D. J. and Heggs, P. J. 1989. Recirculating combined convection in laminar pipe flow. *ASME J. Heat Transfer*, **111**, 106–113

Ostrach, S. 1954. Combined natural- and forced-convection laminar flows and heat transfer of fluids with and without heat sources, in channels with linearly varying wall temperatures. *NACA Tech. Note 3141*, NASA, Washington, DC

Özişik, M. N. 1985. *Heat Transfer, A Basic Approach.* McGraw-Hill, New York

Penot, F. and Dalbert, A.-M. 1983. Convection naturelle mixte et forcée dans un thermosiphon vertical chauffe à flux constant. *Int. J. Heat Mass Transfer*, **26** (1), 1639–1647

Press, W. H., Flannery, B. P., Teukolsky, S. A. and Vetterling, W. T. 1986. *Numerical Recipes—The Art of Scientific Computing.* Cambridge University Press, Cambridge

Reyhner, T. A. and Flügge-Lotz, I. 1968. The interaction of a shock wave with a laminar boundary layer. *Int. J. Nonlinear Mech.*, **3**, 173–199

Rokerya, M. S. and Iqbal, M. 1971. The effects of viscous dissipation on combined free and forced convection through vertical concentric annuli. *Int. J. Heat Mass Transfer*, **14**, 491–495

Scheele, G. F. and Hanratty, T. J. 1962. Effect of natural convection on stability of flow in a vertical pipe. *J. Fluid Mech.*, **14**, 244–256

Shah, R. K. and London, A. L. 1978. Laminar flow forced convection in ducts. *Adv. Heat Transfer*, Supplement 1. Academic Press, London

Sherwin, K. and Wallis, J. D. 1971. Combined natural and forced convection for upflow through heated vertical annuli. *Symp. Heat Mass Transfer by Combined Force and Natural Convection* (I.Mech.E.), Manchester, UK

Sherwin, K. 1968. Laminar convection in uniformly heated vertical annuli. *Br. Chem. Eng.*, **13** (11), 569–574

Sparrow, E. M., Chrysler, G. M. and Azevedo, L. F. 1984. Observed flow reversals and measure-predicted Nusselt numbers for natural convection in a one-sided heated vertical channel. *ASME J. Heat Transfer*, **106**, 325–332

Williams, P. G. 1975. A reverse flow computation in the theory of self induced separation. *Lecture Notes in Physics*, **35**, 445–451

Yao, L. S. 1983. Free and forced convection in the entry region of a heated vertical channel. *Int. J. Heat Mass Transfer*, **26** (1), 65–72

Yao, L. S. 1987. Is fully-developed and non-isothermal flow possible in a vertical pipe? *Int. J. Heat Mass Transfer*, **30** (4), 707–716